Biochemistry

pubs.acs.org/biochemistry Article

Structural and Functional Characterization of a Novel Class A Flavin Monooxygenase from *Bacillus niacini*

Brian C. Richardson,[⊥] Zachary R. Turlington,[⊥] Sofia Vaz Ferreira de Macedo, Sara K. Phillips, Kay Perry, Savannah G. Brancato, Emmalee W. Cooke, Jonathan R. Gwilt, Morgan A. Dasovich, Andrew J. Roering, Francis M. Rossi, Mark J. Snider, Jarrod B. French, and Katherine A. Hicks*

Cite This: *Biochemistry* 2024, 63, 2506−2516 Read Online

ACCESS | Metrics & More | Article Recommendations | Supporting Information

ABSTRACT: A gene cluster responsible for the degradation of nicotinic acid (NA) in *Bacillus niacini* has recently been identified, and the structures and functions of the resulting enzymes are currently being evaluated to establish pathway intermediates. One of the genes within this cluster encodes a flavin monooxygenase (BnFMO) that is hypothesized to catalyze a hydroxylation reaction. Kinetic analyses of the recombinantly purified BnFMO suggest that this enzyme catalyzes the hydroxylation of 2,6-dihydroxynicotinic acid (2,6-DHNA) or 2,6-dihydroxypyridine (2,6-DHP), which is formed spontaneously by the decarboxylation of 2,6-DHNA. To understand the details of this hydroxylation reaction, we determined the structure of BnFMO using a multimodel approach combining protein X-ray crystallography and cryo-electron microscopy (cryo-EM). A liganded BnFMO cryo-EM structure was obtained in the presence of 2,6-DHP, allowing us to make predictions about potential catalytic residues. The structural data demonstrate that BnFMO is trimeric, which is unusual for Class A flavin monooxygenases. In both the electron density and coulomb potential maps, a region at the trimeric interface was observed that was consistent with and modeled as lipid molecules. High-resolution mass spectral analysis suggests that there is a mixture of phosphatidylethanolamine and phosphatidylglycerol lipids present. Together, these data provide insights into the molecular details of the central hydroxylation reaction unique to the aerobic degradation of NA in *Bacillus niacini*.

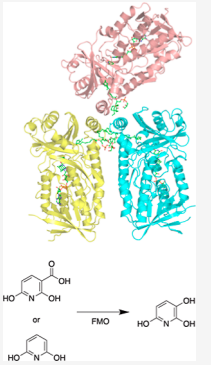

INTRODUCTION

N-Heterocyclic aromatic compounds (*N*HACs) are emerging environmental pollutants. These compounds are known to exhibit toxic effects in plants[1] and aquatic life,[2] yet little is known about how they are absorbed and transported in the soil, and the systemic environmental effects of these molecules are still not well-studied.[3−5] The ubiquitously metabolized nicotinic acid (NA; vitamin B3 or niacin) is a useful model compound for understanding *N*HAC degradation, making it an attractive target for investigating the enzymology of bioremediation principles.[6,7] Notably, the pathway for NA catabolism in anaerobic bacteria is shared by the soil bacteria *Eubacterium barkeri*[8] and *Azorhizobium caulinodans*.[9,10] In aerobic bacteria, two pathways have been described for the degradation of NA. These pathways, characterized in detail in *Pseudomonas*[11] and *Bordetella*[12] species, require six enzyme-catalyzed steps to transform NA to fumaric acid (Figure 1).

A *Bacillus* species that could survive on NA as its sole carbon source was first described in the 1940s.[13] Later work in the 1960s and 70s focused on measuring the accumulation of pathway intermediates and assigning enzymatic reactions. This early work hypothesized that NA was enzymatically converted to 2,6-dihydroxynicotinic acid (2,6-DHNA) via a 6-hydroxynicotinic acid (6-HNA) intermediate by two dehydroxygenaes.[14,15] This alternative pathway for NA degradation in a *Bacillus* species, first proposed by Ensign and Rittenberg,[14] is shown in blue in Figure 1. Decades later, the genome for this NA-degrading bacteria, *Bacillus niacini* DSM 2923 or *Neobacillus niacini*, was annotated and deposited in GenBank.[16,17] This alternative pathway differs from the canonical pathway described in *Pseudomonas*[11] and *Bordetella*[12] in several ways. Most notably, the apparent use of 2,6-DHNA and 2,3,6-trihydroxylated pyridine (2,3,6-THP) as pathway intermediates is unique to the *B. niacini* NA pathway; to date, a 2,6-DHNA metabolite has not been identified or predicted in any other characterized pathway.[18,19] Initial studies of *B. niacini* noted that the bacteria would accumulate the 2,6-DHNA metabolite, and therefore it was hypothesized that the enzymes responsible for the conversion of 2,6-DHNA to 2,3,6-THP might be the rate-limiting steps in the catabolic pathway.[14]

Within the hypothesized gene cluster that encodes for the enzymes of NA degradation in *B. niacini* is a flavin monooxygenase (FMO; WP_063252926; UP10007AB3525). The NA degradation pathways in *Pseudomonas putida* and *Bordetella bronchiseptica*[20−22] also involve a Class A FMO,

Received: June 4, 2024
Revised: August 22, 2024
Accepted: August 27, 2024
Published: September 12, 2024

https://doi.org/10.1021/acs.biochem.4c00306
Biochemistry 2024, 63, 2506−2516

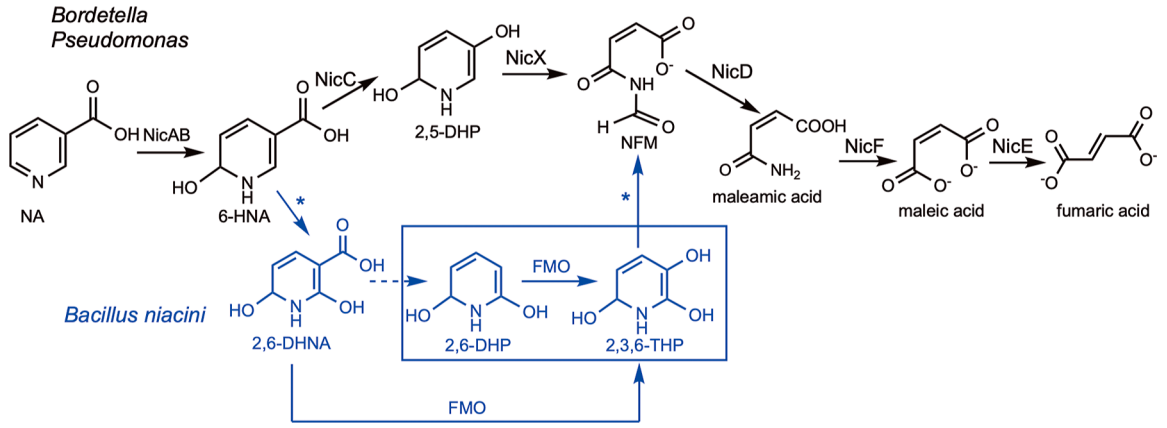

Figure 1. NA degradation pathway in aerobic bacteria (*e.g.*, *Pseudomonas putida* and *Bordetella bronchiseptica* RB50) and a proposed catabolic pathway in *Bacillus niacini*. The reaction catalyzed by the BnFMO is highlighted. Nicotinic acid (NA); 6-HNA (6-hydroxynicotinic acid); 2,5-dihydroxypyridine (2,5-DHP); *N*-formylmaleamate (NFM); maleamic acid; maleic acid; fumaric acid; 2,6-dihydroxynicotinic acid (2,6-DHNA); 2,6-dihydroxypyrdine (2,6-DHP); and 2,3,6-trihydroxypyridine (2,3,6-THP). The dotted line indicates that this process can occur nonenzymatically. The *B. niacini* pathway is emphasized in blue. The asterisks indicate metabolic steps in which the responsible enzymes are under investigation.

NicC, that catalyzes the conversion of 6-HNA to 2,5-dihydroxypyridine (2,5-DHP).[20−22] Here, we demonstrate that the recombinantly expressed *B. niacini* enzyme is an FAD-dependent monooxygenase that does not use 6-HNA as a substrate but accepts either 2,6-DHNA or its decarboxylated counterpart, 2,6-dihydroxypyridine (2,6-DHP), as substrates. To further investigate its biochemical mechanism, we determined the crystal structure of BnFMO, as well as the cryo-electron microscopy (cryo-EM) structure in the presence and absence of 2,6-DHP. These structures place BnFMO in the Class A flavin monooxygenase subfamily.[23,24] Taken together, these data enable the structural and biochemical characterization of BnFMO and provide insights into its novel role in the degradation of NA.

MATERIALS AND METHODS

Synthesis of the *Bacillus niacini* FMO Gene. The BnFMO gene was annotated as a flavin monooxygenase.[25] The gene was synthesized by GenScript (Piscataway, New Jersey), codon optimized for bacterial expression in *E. coli*, and subcloned into the pET-24a(+)-TEV vector. The gene sequence of the resulting construct was verified by DNA sequencing.

BnFMO Overexpression and Purification. Recombinant wild-type, selenomethionine (SeMet)-substituted BnFMO was overexpressed and purified by using standard methods. *E. coli* B834(DE3) cells were transformed with the BnFMO plasmid and grown overnight at 37 °C on Luria Broth (LB) plates containing kanamycin (50 μg/mL). A single colony was used to inoculate a starter culture containing 15 mL of LB and 50 μg/mL kanamycin. The next morning, large cultures (1 L) were grown using minimal media supplemented with 1× M9 minimal salts, 20 mg/L of all amino acids except methionine, 50 mg/L L-selenomethionine, 1× MEM vitamin mix, 0.4% glucose, 2 mM $MgSO_4$, 0.1 mM $CaCl_2$, 25 mg/L $FeSO_4$, and 25 μg/mL kanamycin. Cells were grown with shaking at 37 °C until the OD_{600} was between 0.6 and 0.8, and the temperature was then lowered to 15 °C. After a 45 min incubation at 15 °C, protein expression was induced with 1 mM isopropyl β-D-thiogalacto-pyranoside (IPTG). Cells were harvested at 6,000*g*, and the resulting cell pellet was stored at −80 °C prior to purification.

SeMet BnFMO was obtained from ∼ 9 g of cell pellet from 2 L of culture. The cell pellet was resuspended in ∼ 40 mL of cold binding buffer [20 mM Tris (pH 8.0), 500 mM NaCl, and 3 mM β-mercaptoethanol]. Approximately 20 mg of flavin adenine dinucleotide (FAD) was added to the resuspended cells. Cells were lysed on ice by sonication using a pulse sequence of 1 s on, 3 s off, for 1 min total, which was repeated three times. The cellular debris was removed via centrifugation at 40,000*g* for 30 min at 4 °C. The resulting clarified lysate was added over a 4 mL Ni-NTA column (GE Life Sciences) pre-equilibrated with lysis buffer. The column was then washed with ∼ 100 mL of lysis buffer to remove nonspecific protein binders. A stepwise elution of imidazole was then used to elute SeMet BnFMO from the column. This gradient consisted of 20 mL of lysis buffer supplemented with 25 mM imidazole, 10 mL of lysis buffer supplemented with 50 mM imidazole, and 20 mL of lysis buffer containing 250 mM imidazole. After nickel affinity chromatography, the BnFMO protein was further purified using size exclusion chromatography (HiLoad 26/60 Superdex 200 pg, GE Healthcare) using a running buffer consisting of 20 mM Tris-HCl (pH 8.0), 50 mM NaCl, and 1 mM DTT. Aliquots of the resulting fractions were analyzed by SDS-PAGE and fractions deemed to be >95% pure were combined. The final SeMet BnFMO sample was greater than 95% pure based on SDS-PAGE. The resulting sample was bright yellow in color and was concentrated to 12−13 mg/mL based on absorbance at 280 nm. The protein was aliquoted, flash frozen, and stored at −80 °C for crystallization trials.

The native BnFMO protein was overexpressed in BL21-(DE3) cells grown in LB medium containing kanamycin (50 μg/mL) and was purified as described above. Samples were concentrated to approximately 10 mg/mL, flash frozen, and stored at −80 °C for cryo-EM trials.

Native BnFMO was also purified for use in kinetic and biochemical assays. This protein was overexpressed as described above and purified by nickel affinity chromatography only. Samples were buffer-exchanged into a storage buffer containing 10 mM Tris (pH 7.2), 1 mM DTT, and 25% glycerol. Samples were concentrated to approximately 100 μM,

https://doi.org/10.1021/acs.biochem.4c00306
Biochemistry 2024, 63, 2506−2516

flash frozen, and stored at −80 °C for biochemical characterization. Prior to biochemical experiments, the protein samples were thawed and buffer-exchanged into 10 mM Tris (pH 7.2) to remove the storage buffer. The protein concentration was then remeasured and concentrated to approximately 100 μM.

Cryo-EM Data Sample Preparation and Collection. The SeMet BnFMO sample prepared as described above without 2,6-DHP was diluted to between approximately 0.2 and 1 mg/mL in a buffer consisting of 50 mM Tris (pH 8.0) and 150 mM NaCl. These samples were applied to a 300 mesh copper C-flat grid (Electron Microscopy Sciences) and blotted and vitrified with a Vitrobot Mark IV (Thermo Fisher) with a blotting time of 4 s and blotting force of 0 with >90% humidity at 4 °C. Using CryoSPARC,[26] 2.9 million particles were extracted from 4568 super-resolution movies collected on a Krios G4 with Falcon 4i detector and filtered by serial 2D classification to a final set of 433,941 particles. Homogenous refinement in C1 symmetry yielded an estimated resolution of 2.5 Å; sharpening with a *B*-factor of −65 Å^2 and applying local resolution filtering generated the final map used for model refinement in Phenix.

To generate the 2,6-DHP-bound sample, 12 mg/mL of wild-type FMO (80 μM) was incubated with 1.5 mM FAD and 2.5 mM 2,6-DHP overnight at 4 °C. The sample was diluted to 0.9 mg/mL in 20 mM Tris 8 and 50 mM NaCl before being applied to Quantifoil Au grids. Images were collected on a Titan Krios with a Gatan K3 detector with a super-resolution pixel size of 0.6637 Å. Using CryoSPARC, an initial set of 3.0 million particles were picked via template and extracted from 7048 micrographs; after serial 2D classification and removal of an additional 397 exposures with questionable particles, an optimal set of 1.3 million particles produced a map with an estimated resolution of 2.8 Å after homogeneous refinement in C1. Sharpening with a *B*-factor of −95 Å^2 and filtering by local resolution generated the map used for model refinement in Phenix. The final models have statistics appropriate for their resolution as determined by MolProbity,[27] EMringer,[28] and MapQ (Table S1 and Figure S1).

Synthesis of 2,6-Dihydroxynicotinic Acid. A 50 mL round-bottom flask equipped with a stir bar was charged with 2,6-dimethoxynicotinic acid (1.00 g, 6.61 mmol, 1 equiv) and was attached to a reflux condenser and purged with N_2 for 15 min. HBr (16 mL, 33% by weight, 281 mmol, 42 equiv) was added, and the solution was allowed to react at 50 °C for 16 h. After 16 h, the solution was allowed to cool, and diethyl ether (32 mL) was added to the dark red solution. N_2 was blown over the solution to induce evaporation, and the solution was evaporated to dryness. The product was collected as a mixture of starting material and other byproducts. The product was purified by trituration with ethyl alcohol to afford an off-white solid (0.152 g, 15%). NMR spectra were obtained on a Bruker Avance 300 MHz NMR spectrometer (300.6 MHz ^{1}H reference frequency and 75.6 MHz for ^{13}C) equipped with a SB broadband probe in DMSO-d_6 as the solvent, unless otherwise noted, and referenced to the residual solvent peak. NMR spectra were processed and baseline-corrected using MestreLabs MNOVA software packages. ^{1}H NMR (300 MHz), δ 8.03 (d, 1H) 5.87 (d, 1H). ^{13}C NMR (75 MHz), δ 167.7, 165.4, 163.0, 146.3, 97.4. The ^{1}H and ^{13}C NMR spectra of 2,6-DHNA are shown in Figure S2. The stability of 2,6-DHNA was monitored by ^{1}H NMR spectroscopy for a period of 106 h by obtaining NMR spectra of the same sample at regular intervals (Figure S3).

BnFMO Steady-State Kinetic Assay. Steady-state kinetic analysis of BnFMO was conducted by measuring the initial rates of NADH oxidation in an assay buffer consisting of 0.1 M Tris (pH 7.50) in a 96-well plate using a Synergy HT microplate reader (BioTek). Initial kinetic assays were done using a 20 mM substrate/substrate analogue and 100 nM wild-type BnFMO. Reactions were initiated by the addition of 1.5 mM NADH, and the kinetics of the reaction were monitored at 285 nm as this wavelength had the highest signal. The reactions were monitored every 30 s for 30 min. No activity was observed with NADPH, so this coenzyme was not assayed. The activity was tested using a variety of potential substrates including the following: 2,6-DHP, 2,6-DHNA, 6-HNA, 2,4-dihydroxybenzoic acid (2,4-DHBA), and resorcinol. Substrates were solubilized in DMSO. Data were analyzed using an extinction coefficient of $\varepsilon = 3.808\ \mathrm{mM^{-1}\ cm^{-1}}$.

Substrates that demonstrated activity in the initial assay were further analyzed at varying substrate concentrations (50 μM−10 mM) with a constant concentration of BnFMO (100 nM) and NADH (1 mM). The background rate of NADH oxidation was subtracted from all of the data. The initial rate of NADH oxidation (∼10% of the reaction) was plotted against substrate concentration, and the data were fit to eq 1 using KaleidaGraph (Synergy Software) to obtain steady-state kinetic parameters.

$$v = \frac{(V_{max}[S])}{K_m + [S]} \quad (1)$$

Figure Preparation. Figures were generated using the PyMOL molecular graphics system, version 2.5 (Schrödinger, LLC), Chimera (UCSF),[29] and ChemDraw (CambridgeSoft).

RESULTS AND DISCUSSION

Genetic and Biochemical Properties of BnFMO. Based on primary sequence analysis, the BnFMO gene is an FAD-dependent oxidoreductase that contains an FAD-binding domain.[30] The resulting enzyme was bright yellow following gel filtration chromatography, indicative of flavin binding, even when FAD was not added during purification. High-performance liquid chromatography (HPLC) analysis indicates that the BnFMO coenzyme was FAD rather than flavin adenine mononucleotide (FMN) (Figure S4).

Catalytic Activity of BnFMO. The catalytic activity of the BnFMO was measured with several potential substrates including 2,6-DHP, 2,6-DHNA, 6-HNA, 2,4-DHBA, and resorcinol by monitoring the rate of NADH oxidation.[20] Previous studies have demonstrated the halide ions can inhibit catalysis for Class A flavin monooxygenases, so halide ions were not included in the BnFMO storage buffer or assay buffer.[20,31,32] BnFMO catalytic activity was detected with both 2,6-DHP and 2,6-DHNA with a slight preference for 2,6-DHNA based on the measured specificity constant (Table 1). 2,6-DHNA is the predicted substrate for BnFMO based on previous work.[14] This study noted that the *Bacillus* species accumulated 2,6-DHNA.[14] The measured specificity constant for 2,6-DHNA is relatively low ($10^2\ \mathrm{M^{-1}\ s^{-1}}$) in comparison to other Class A flavin monooxygenases, which correlates with this observation. Specificity constants for this enzyme superfamily range from $10^4\ \mathrm{M^{-1}\ s^{-1}}$ for the related *P. putida* NicC,[20] which is involved in NA metabolism, to $10^6\ \mathrm{M^{-1}\ s^{-1}}$ for *Klebsiella pneumoniae* HpxO,[16] an enzyme in uric acid metabolism. Together, these studies suggest that the FMO-

https://doi.org/10.1021/acs.biochem.4c00306
Biochemistry 2024, 63, 2506−2516

Table 1. Steady-State Kinetic Parameters for the Reactions Catalyzed by the Wild-Type BnFMO

substrate[a]	$V_{max}/[E]$ (s^{-1})	K_M^S (mM)[b]	k_{cat}/K_M^S (M^{-1} s^{-1})
2,6-DHP	0.42 ± 0.02	3.4 ± 0.4	(1.2 ± 0.2) × 10^2
2,6-DHNA	1.30 ± 0.05	5.5 ± 0.4	(2.4 ± 0.1) × 10^2
6-HNA	NA[c]	NA	NA
2,4-DHBA	NA	NA	NA
resorcinol	NA	NA	NA

[a]The concentration of NADH was saturating. [b]With respect to the substrate: 2,6-DHP, 2,6-DHNA, 6-HNA, 2,4-DHBA, or resorcinol. [c]NA: no activity. Activity was below the detection limit of the assay.

catalyzed step is the rate-limiting step in NA metabolism in *B. niacini*.

2,6-DHNA is highly labile in solution and begins to undergo spontaneous, nonenzymatic decarboxylation in solution to 2,6-DHP within 30 min with complete conversion within ~ 100 h (Figure S3). This decarboxylation results in a change in the splitting pattern observed in the aromatic region of the ^{1}H NMR spectrum: two downfield doublets at δ 5.82 and 7.98 begin to decrease in intensity during the conversion, and a new triplet peak appears at 7.50 ppm. These changes are indicative of a molecule undergoing a decarboxylation event. This instability of 2,6-DHNA suggests that the BnFMO can accept both a carboxylated and decarboxylated hydroxylated pyridine as its substrate. This is consistent with the known function of most Class A flavin monooxygenases that act upon unsubstituted carbons.[33] These data allow for positioning BnFMO midway through the overall NA degradation pathway shown in Figure 1.

Summary of Structural Data. We have determined a series of BnFMO structures including a crystal structure of SeMet BnFMO with clear evidence for FAD binding in at least one chain (PDB ID: 8UIU), a cryo-EM structure of SeMet BnFMO with FAD bound to all chains (PDB ID: 8URC), and a cryo-EM structure of native BnFMO with FAD and 2,6-DHP bound to all chains (PDB ID: 8URD; Tables S1 and S2). Cryo-EM electrostatic potential maps were determined to an estimated overall resolution (FSC = 0.143) of 2.5 Å (in the absence of the 2,6-DHP ligand) and 2.8 Å (2,6-DHP bound), as shown in Figure S5. Water molecules were not modeled into any of the structural models. As the cryo-EM structures have higher resolution and maps that allowed unambiguous placement of the ligand and coenzyme density in all three chains, we have focused our discussion below of the BnFMO structure on these data. Information about the crystal structure is provided in the Supporting Information as it provides important details on the FMO oligomeric structure.

Overall BnFMO Structure. The BnFMO protomer (Figure 2A) has a α/β tertiary structure similar to other Class A flavin monooxygenases, of which the best characterized is *p*-hydroxybenzoate hydroxylase.[34−36] The first 4−6 residues of each protomer chain were disordered and are not included in the final model. The overall protomer structure is shown in Figure 2A. Like other Class A flavin monooxygenases, BnFMO consists of three domains. The N-terminal domain contains a parallel five-stranded β-sheet (β9↑β17↑ β1↑β2↑β5↑), four α-helices, and a three-stranded antiparallel β sheet (β6↓β7↑β8↑). Most of the FAD-protein interactions are made with the N-terminal domain. A second domain consists of a mainly antiparallel, seven-stranded β sheet (β4↓β3↑β12↑β13↓β14↑ β11↓β15↓), a two-stranded antiparallel β-sheet (↓β16↑β10), and five shortα-helices. This domain contains most of the residues in the 2,6-DHP- and lipid-binding sites. The C-

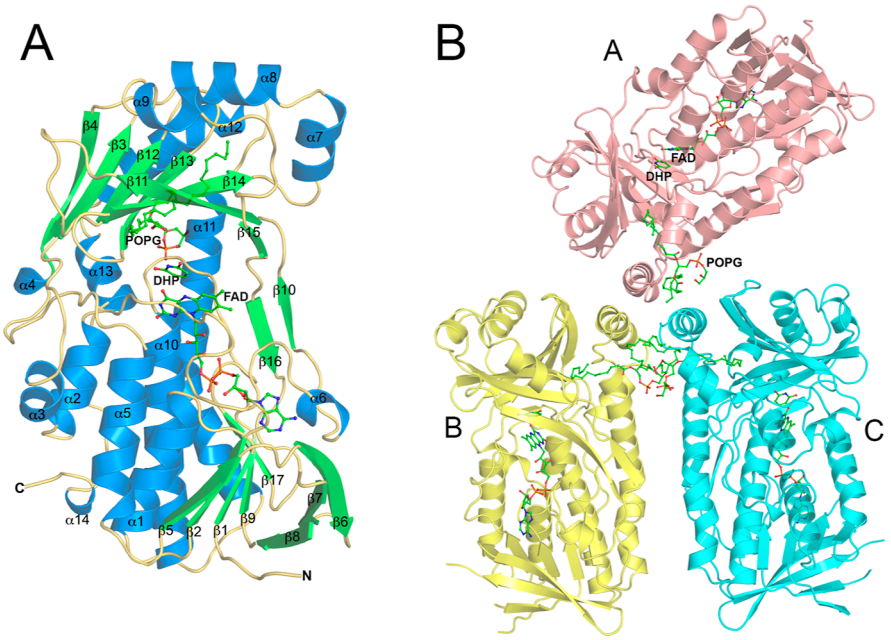

Figure 2. BnFMO structure based on cryo-EM data. (A) Ribbon diagram of one protomer of BnFMO with secondary structural elements labeled. The α-helices are shown in blue, the β-strands are shown in green, and the loops are colored yellow. The bound FAD cofactor, 2,6-DHP ligand (labeled DHP), and a 1-cis-9-octadecanoyl-2-cis-9-hexadecanoylphosphatidyl glycerol lipid molecule (labeled POPG) (colored by element) are shown in ball-and-stick representation. Carbon atoms are in green, oxygen atoms in red, phosphorus atoms in orange, and nitrogen atoms in blue. (B) Overall trimeric structure of BnFMO (colored by chain). Shown in ball-and-stick representation are the FAD, 2,6-DHP (labeled DHP), and lipid molecules (labeled POPG). Atomic color scheme as in panel A. The ligand and FAD coenzyme are labeled in chain A only for clarity. Chains are labeled with chain A shown in salmon, chain B in yellow, and chain C in cyan.

https://doi.org/10.1021/acs.biochem.4c00306
Biochemistry 2024, 63, 2506−2516

terminal domain comprises four short α-helices and two long α-helices.

While PDBePISA[37] does not predict that the BnFMO protein forms a higher-order structure, we confirmed the oligomeric state based on analytical ultracentrifugation (Figure S6) and size exclusion chromatography (Figure S7), as well as observing the interface in the orthogonal structural techniques of crystallography (Figure S8) and cryo-EM.[37] This trimeric structure makes BnFMO distinctive as Class A flavin monooxygenases are typically monomeric.[16,35,38] The observed interface is not perfectly symmetrical as it is organized through two separate pseudosymmetries rather than a single 3-fold rotation axis (Figures 2B and 3), resembling a Y-shape with

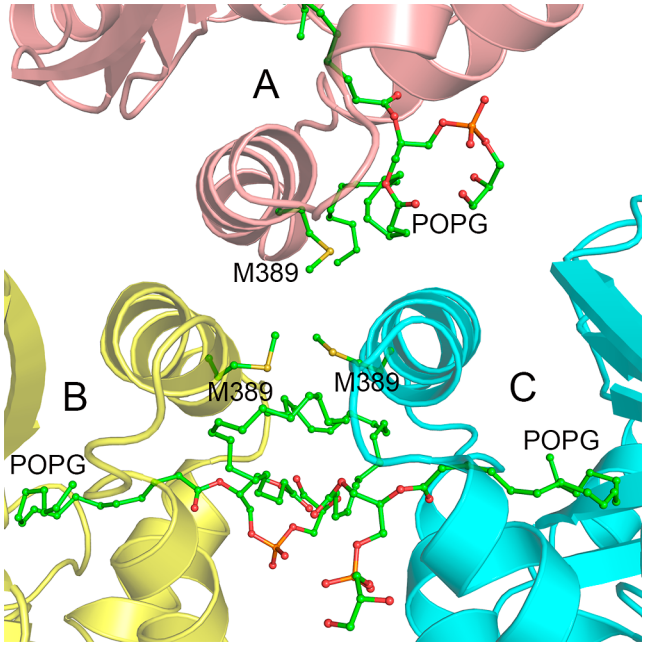

Figure 3. BnFMO trimeric interface. There are lipids present at the trimeric interface that have been modeled in as the phospholipid 1-cis-9-octadecanoyl-2-cis-9-hexadecanoylphosphatidyl glycerol lipid molecule (labeled POPG; PDB ID: DR9). There is also a set of methionine residues (M389 from each chain) that make contact at the oligomeric interface. Chain coloring as in Figure 2 with chain A shown in salmon, chain B in yellow, and chain C in cyan. The bound lipid and Met389 are shown in ball-and-stick representation colored by the element. Oxygen atoms are shown in red, sulfur atoms in yellow, phosphorus atoms in orange, and carbon atoms in green.

chains B and C closer to each other than to chain A. Also present at the trimeric interface is nonprotein density/potential similar to what was observed at the dimer interfaces of the flavoenzymes 3-hydroxybenzoate 6-hydroxylase (3HB6H; E.C. 1.13.14.26; PDB ID: 4BJZ)[39] and 6-hydroxy-L-nicotine oxidase (6HLNO; E.C. 1.5.3.5; PDB ID: 3K7Q).[40] In the 3HB6H structure, these lipids were determined to be phosphatidylinositol and were hypothesized to be important for maintaining the dimeric structure and substrate orientation.[39,41] The lipids in 6HLNO were modeled as diacylglycerophospholipid; however, the biological function of these lipid molecules remains unknown.[40] Speculated functions for these lipids are to restrain domain motions during the conformational changes that occur during catalysis or to stabilize interactions between the substrate-binding domains and the lipid bilayer.[42] To determine the possible identity of the lipid at the trimeric interface, high-resolution mass spectrometry (MS) was performed. These MS results are consistent with the presence of a heterogeneous mixture of phosphatidylethanolamine (PE) and phosphatidylglycerol (PG) phospholipids associated with FMO (Figure S9). As the resolution of the structures precluded definitive assignment, we have modeled the lipids, in accordance with the strongest MS peak, as a PG: 1-cis-9-octadecanoyl-2-cis-9-hexadecanoylphosphatidyl glycerol (POPG; PDB ID: DR9; Table S3 and Figures S10 and S11). The cryo-EM and Polder omit maps from the crystallographic data (Figure S12) support the modeling of the POPG lipid at the oligomeric interface, as does the Q-score analysis of both cryo-EM maps.[43] In particular, the omit maps show clear electron density for a phospholipid headgroup (Figure S12C,D). One of the lipid molecule's two tails is inserted into the core of the protein, coming within 10 Å of the active site, and the other lies at the protein−protein interface, potentially stabilizing it. There are also methionine residues from each chain, Met389, that make contact at the oligomeric interface and may also be involved in oligomeric stabilization (Figure 3).

While the functional relevance of the atypical structure of BnFMO is unclear, protein oligomers often have several benefits over monomeric proteins, including larger binding surfaces and the capacity to form an active site at the oligomeric interface.[44,45] BnFMO oligomerization could enable additional protein−protein interactions or regulatory activities (Figure 2B). As the BnFMO active site is approximately 28 Å from the trimeric interface, it is possible that this nonsymmetrical interface could allow for other protein(s) in the *B. niacini* NA metabolic pathway (Figure 1) to bind. Finally, it is possible that the oligomerization and lipid binding act together to modify or regulate activity.

As has been observed with other Class A flavin monooxygenases, such as MHPCO,[38] 3-hydroxybenzoate hydroxylase (MHBH),[38] and HpxO,[16] there is a tunnel that leads from the surface to the active site (Figure 4A), approximately 16 Å in length and 14 Å in width. Several

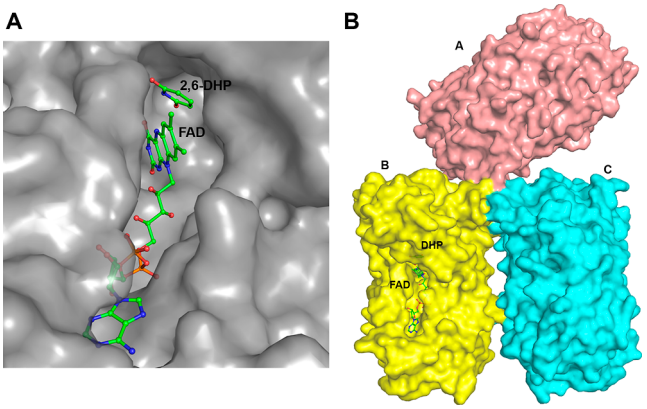

Figure 4. Surface representation of the tunnel leading to the BnFMO active site. (A) FAD and 2,6-DHP are shown in ball-and-stick representation with green carbon atoms, red oxygen atoms, blue nitrogen atoms, and orange phosphorus atoms in chain B. (B) Overall structure of BnFMO with chains shown in a space filling model with chain A in salmon, chain B in yellow, and chain C in cyan. The tunnel leading to the active site is highlighted in chain B (yellow). The FAD coenzyme and 2,6-DHP (labeled DHP) ligand are colored as in panel A.

https://doi.org/10.1021/acs.biochem.4c00306
Biochemistry 2024, 63, 2506−2516

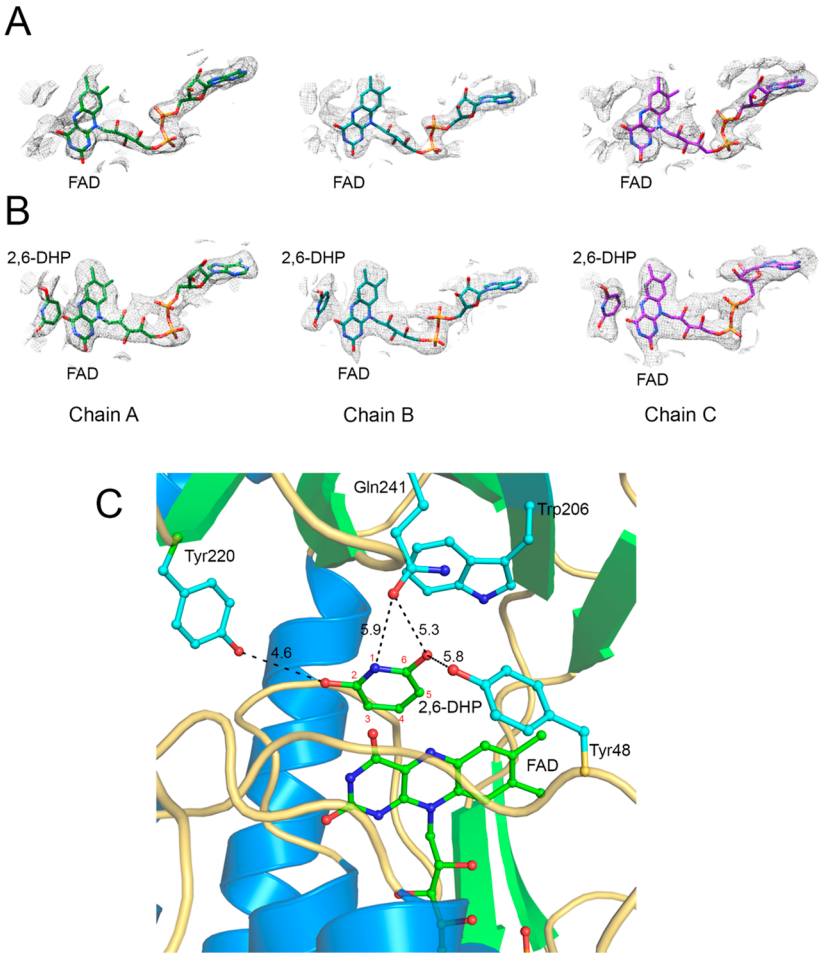

Figure 5. BnFMO active site. (A,B) Cryo-EM maps within 2.3 Å of FAD and 2,6-DHP are shown for ligands associated with each chain contoured to 0.358 (panel A; without 2,6-DHP) or 0.131 (panel B; with 2,6-DHP) to show similar maps for the adenine and phosphate groups well-resolved in both structures. (C) 2,6-DHP binding site. The oxygen atoms are shown in red, the phosphorus atoms are in orange, and the nitrogen atoms are shown in blue. The carbon atoms for 2,6-DHP and FAD are shown in green, while the protein side chain carbon atoms are shown in cyan. Distances are shown with black numbers in Angstrom (Å). Red numbers refer to the atomic numbering of the 2,6-DHP ligand.

hydrophobic residues are part of the tunnel, including Val366, Leu275, and Trp273. The relatively large size of this tunnel could account for the substrate specificity of BnFMO, which can accept both 2,6-DHP and 2,6-DHNA as a substrate. The location of the tunnel relative to the overall structure is highlighted in Figure 4for chain B (shown in yellow). It is conceivable that in the large space between chains A and B another protein binds, allowing for metabolite channeling.

Active Site and Coenzyme Binding Sites. Each BnFMO chain contains well-resolved density representing the adenine and phosphate moieties of bound FAD. Addition of 2,6-DHP resolves the isoalloxazine moiety and introduces a new signal nearby corresponding to the 2,6-DHP ligand itself (Figure 5A,B), validated by Q-scores of both 2,6-DHP and improved FAD (Table S4). The cryo-EM map with the best fit to density, as estimated by Q-scores,[43] or the 2,6-DHP ligand in chain B demonstrates evidence of 2,6-DHP binding and the approximate orientation of the aromatic ring and hydroxyl groups at the C2 and C6 positions (Figure S13). Due to the lack of direct evidence of the ionization state of the C2 and C6 hydroxyls of 2,6-DHP, these functional groups were modeled in their neutral forms, and the ligand is modeled as the enol tautomer. The BnFMO active site thus contains the isoalloxazine ring of the FAD coenzyme as well as 2,6-DHP, which is one of the FMO substrates. Comparison of the BnFMO active site to those of other Class A flavin monooxygenases reveals several structural similarities. Members of the Class A flavin monooxygenase family all contain a conserved proline residue near the isoalloxazine ring of FAD (Pro317 in BnFMO). The Class A flavin monooxygenase active sites typically also contain several hydrophobic, aromatic residues; here, the BnFMO active site contains a tryptophan residue (Trp206) located near the 2,6-DHP binding site and two tyrosine residues (Tyr48 and Tyr220; Figure 5C). For clarity, this figure shows only the 2,6-DHP binding site in chain A and does not show the lipid molecule. The BnFMO active site has several potential hydrogen bond donors and acceptors, including Tyr48 and Tyr220 hydroxyls and the Gln241 amide. While the observed distances are not within range of hydrogen bonding to 2,6-DHP specifically, 2,6-DHP is only one of several substrates for BnFMO (Table 1), and these residues may contribute to the enzyme's broader activity. Alternatively, as the resolution of the map is insufficient to model water molecules, these residues may act in a solvent network.

A series of tyrosine residues have also been proposed to be catalytically relevant in the PHBH mechanism,[46−48] and a histidine/tyrosine dyad has been proposed to be the catalytic residues in the related NA-degrading enzyme, NicC.[20−22] Due

https://doi.org/10.1021/acs.biochem.4c00306
Biochemistry 2024, 63, 2506−2516

to the symmetry of the 2,6-DHP ligand, it is possible that either C3 or C5 becomes hydroxylated, leading to the formation of the 2,3,6-THP product (Figure 5C). In this structure, both the C3 and C5 atoms of 2,6-DHP are within the expected distance of the C4a atom of the FAD isoalloxazine ring, the site of hydroxyl transfer. Specifically, the C3 atom is located 3.9 Å from the C4a carbon of the FAD isoalloxazine ring, and the C5 atom is 3.7 Å from the C4a atom. These distances are within the expected distance for hydroxylation from the FAD hydroperoxyflavin intermediate.[16,38] Furthermore, Trp206 is well-positioned to be involved in parallel displaced $\pi-\pi$ stacking, as has been observed in other Class A flavin monooxygenases.[16,38]

Studies primarily on PHBH have shown that the isoalloxazine ring of FAD changes conformations during catalysis from an "out"[34] to an "in"[35] to an "open"[36] conformation. The flavin is reduced by NADH in the "out" conformation (PDB ID: 1PBF).[34] The flavin then moves to the "in" conformation during catalysis when the substrate is hydroxylated by the flavin hydroperoxide (PDB ID: 1PBE).[35] Finally, the flavin moves to the "open" conformation (PDB ID: 1K0I),[36] allowing for subsequent substrate binding and product release. Recently, an additional "sliding" conformation was observed for the enzyme PieE, in which the isoalloxazine ring is between the "in" and "out" conformations (PDB ID: 6U0P).[49] In the liganded BnFMO structure, the FAD isoalloxazine ring is in the "in" conformation, indicating that it is in a catalytically active state (Figure 6).[35,50]

While we did not experimentally validate the NADH-binding pocket in these structural studies, it is known that the binding pocket for NADH is well-conserved in Class A flavin monooxygenases.[23,51,52] Based on alignment of BnFMO·2,6-DHP with the structure of the R220Q PHBH·NADH complex (PDB ID: 1K0J),[36] a potential binding pocket for NADH on the protein surface has been identified (Figure S14). In this binding pocket, there are several residues, based on their alignment to residues in R220Q PHBH, that could be involved in binding the NADH coenzyme. These residues include Leu289, Leu290, and Arg183, which are located near the potential position of the adenosyl group of NADH. In addition, Arg292 could be involved in binding interactions with the diphosphate and nicotinamide groups of NADH.

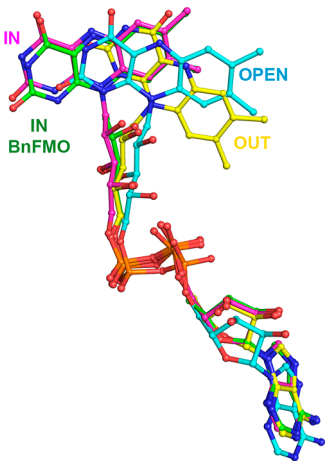

Figure 6. FAD binding site. The FAD molecules are overlaid to highlight the position of the isoalloxazine ring. The FAD molecule is shown in the "open" conformation in R220Q PHBH (PDB ID: 1K0I) complexed with the *p*-hydroxybenzoate (PHB) substrate and shown with cyan carbon atoms. The FAD is in the "out" conformation in PHBH (PDB ID: 1PBF) bound to 2-hydroxy-4-aminobenzoic acid (BHA) and is shown with yellow carbon atoms. The FAD is in the IN conformation in PHBH (PDB ID: 1PBE) complexed with PHB and is depicted with purple carbon atoms. The BnFMO FAD is in the "in" conformation with green carbon atoms. For clarity, only the FAD molecules are shown. Nitrogen atoms are shown in blue, phosphorus atoms in orange, and oxygen atoms in red.

It is possible that Arg294 or Arg292 could be involved in determining whether FMO accepts NADH or NADPH as the reducing agent. In the current 2,6-DHP·FAD·BnFMO model, the side chains of these arginine residues are positioned away from the 2'-atom of NAD(P)H, which it attached to a phosphate in NADPH, but could reorient to form an ionic bonding interaction(s). This is also consistent with our kinetic data (Table 1), where we observed catalysis with a NADH coenzyme. Based on this binding model, the distance between C4 on the nicotinamide ring is ∼ 20 Å from N5 of the flavin isoalloxazine ring. Therefore, similar to what is suggested for PHBH, for the flavin to become reduced, there must be a movement from the FAD ring to the "out" position and a large conformational change in the position of the NADH.[36]

Comparison to Other Class A Flavin Monooxygenases. Based on the results of the distance matrix alignment (DALI) server,[53] BnFMO is structurally most similar to other flavin monooxygenases (Table 2 and Figure 7). Specifically, the enzyme has high structural similarity to *p*-nitrophenol 4-monooxygenase, PnpA (PDB ID: 6AIN),[54] PHBH (PDB ID: 1IUS),[46] fumarylacetoacetate hydrolase (PDB ID: 6FHO),[55] halogenase, PltA (PDB ID: 5DBJ),[56] squalene monooxygenase (PDB ID: 6C6N),[57] a probable FAD-dependent monooxygenase from *Pseudomonas aeruginosa* (PDB ID: 2X3N),[58] and kynurenine 3-monooxygenase (PDB ID: 6FOX).[59]

Interestingly, of the top 999 enzymes identified in the Protein Data Bank (PDB) as structurally similar, *P. putida* NicC, which is also involved in the degradation of NA,[20,21] was number 257 with a *Z*-score of 24.9 and 14% primary sequence identity. In addition, 2,6-dihydroxypyridine-3-hydroxylase (PDB ID: 2VOU), which is involved in nicotine degradation in *Arthrobacter nicotinovorans* and catalyzes the conversion of 2,6-DHP to 2,3,6-THP, has only 14% primary sequence coverage to BnFMO. It was number 214 on the list with a *Z*-score of 25.4.[60]

Mechanistic Implications. The 2,6-DHP ligand-bound BnFMO structure allows us to propose the following hydroxylation mechanism, consistent with similar mechanisms observed for other flavin monooxygenases (Figure 8).[23] Although there do not appear to be any direct interactions between the 2,6-DHP ligand and BnFMO protein residues (Figure 5C), several protein side chains are within ∼ 4−6 A of functional groups on the 2,6-DHP ligand, indicating that there might be a conformational change prior to or during catalysis allowing for product formation. These residues include Tyr48, Tyr220, and Gln241. Of these residues, only Tyr220 is moderately conserved in other Class A flavin monooxygenases predicted to be structurally similar to BnFMO based on DALI analysis (Table 2 and Figure S15). This tyrosine residue is also present in PHBH (PDB ID: 1IUS),[46] fumarylacetoacetate hydrolase (PDB ID: 6FHO),[55] and halogenase, PltA (PDB ID: 5DBJ).[56] In comparison, Gln241 is only conserved in PHBH, and Trp48 is not conserved at all. Trp206, which is involved in parallel displaced $\pi-\pi$ stacking, is conserved in PHBH, halogenase PltA, and the functionally related protein *P. putida*

https://doi.org/10.1021/acs.biochem.4c00306
Biochemistry 2024, 63, 2506−2516

Table 2. Structural Comparison to Other Proteins in the Protein Data Bank[g]

PDB ID[a]	Z-score[b]	rmsd[c]	no. Res.[d]	% ID[e]	description
6AIN	31.9	3.1	348	16	*p*-nitrophenol 4-monooxygenase, PnpA
1IUS	31.9	3.5	351	15	*p*-hydroxybenozoate hydroxylate[f]
6FHO	30.8	3.1	335	19	fumarylacetoacetate hydrolase
5DBJ	30.6	2.9	344	19	halogenase, PltA
6C6N	30.4	2.9	354	18	squalene monooxygenase
2X3N	30.1	3.1	329	19	probable FAD-dependent monooxygenase
6FOX	29.6	2.8	340	18	kynurenine 3-monooxygenase

[a]Protein data bank identifier. [b]The calculated Z-score. [c]Root mean square deviation for the alignment. [d]Number of residues in the structures being compared. [e]Percentage sequence identity. [f]There are many structures of *p*-hydroxybenozoate hydroxylas in the PDB. 1IUS has the highest sequence similarity to BnFMO. [g]Structural alignment of BnFMO to all structures in the PDB as of December 2023. The top 7 of 999 results are given.

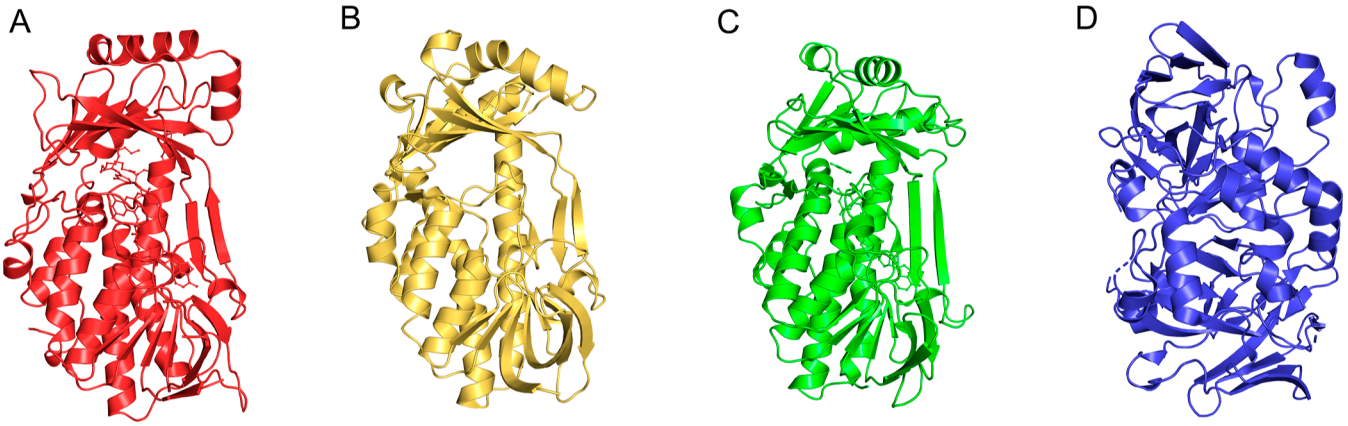

Figure 7. Structural comparison of BnFMO to other class A flavin monooxygenases. The structures are shown in ribbon representation with any bound coenzymes or ligands shown in ball-and-stick representation. (A) BnFMO (PDB ID: 8URD). The structure is shown in red. (B) *p*-nitrophenol 4-monooxygenase, PnpA (PDB ID: 6AIN; Z-score 31.9), is shown in yellow. (C) *p*-Hydroxybenzoate hydroxylase (PHBH; PDB ID: 1IUS; Z-score 31.9) is shown in green. (D) Fumarylacetoacetate hydrolase (PDB ID: 6FHO; Z-score 30.8) is shown in blue.

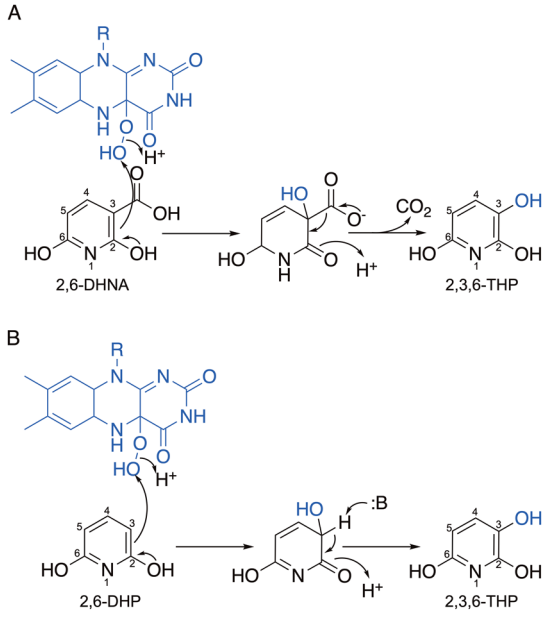

Figure 8. Proposed BnFMO-catalyzed reaction mechanism. (A) Proposed decarboxylative hydroxylation mechanism for the transformation of 2,6-DHNA to 2,3,6-THP. (B) Proposed transformation of the alternative 2,6-DHP substrate to 2,3,6-THP. Based on structural data, Tyr220 likely acts as a general base and deprotonates C2-OH, leading to electrophilic aromatic substitution.

NicC,[20] indicating that it could be important for substrate binding and orientation.

Our proposed mechanism for the BnFMO-catalyzed reaction using 2,6-DHNA as a substrate involves an electrophilic aromatic substitution reaction that begins with electron movement from C2-OH (Figure 8A). This working hypothesis is based on our observation that 6-HNA, which lacks C2-OH, is not a BnFMO substrate (Table 1). It is possible that during catalysis, conformational changes occur, and amino acid residues move closer to the substrate, allowing them to become catalytically essential. In the proposed mechanism, a proton is abstracted from C2-OH by the evolutionarily conserved Tyr220, leading to electrophilic aromatic substitution at C3. Gln241 could be involved in a hydrogen-bonding interaction with 2,6-DHP, leading to increased pyridine ring nucleophilicity. This reaction results in a hydroxylation and rehybridization of C3 similar to what was measured by secondary kinetic isotope effects for NicC.[20] The resulting tetrahedral intermediate is then decarboxylated, re-establishing the aromaticity of the system and leading to the formation of the 2,3,6-THP product. There is space in the active site to accommodate the C3-carboxylate on 2,6-DHNA. This proposed mechanism is similar to the decarboxylative hydroxylation mechanism of the related flavin monooxygenase, NicC, that is also involved in NA metabolism.[20−22]

BnFMO can also utilize 2,6-DHP as a substrate, likely because 2,6-DHNA spontaneously decarboxylates to 2,6-DHP (Figure S3). This potential mechanism is shown in Figure 8B,

https://doi.org/10.1021/acs.biochem.4c00306
Biochemistry 2024, 63, 2506−2516

in a mechanism similar to other flavin monooxygenases, such as PBHB,[46,48,61] that does not involve a decarboxylative hydroxylation but instead the hydroxylation of an unsubstituted carbon atom. Although our kinetic data (Table 1) indicate that 2,6-DHNA is the preferred BnFMO substrate, the kinetic constants are almost identical for the two substrates. To establish the role of protein residues in this catalytic mechanism, future studies will involve the creation of site-directed BnFMO variants guided by residues near the 2,6-DHP binding site (Figure 5C).

In summary, we have structurally characterized a flavin monooxygenase from *B. niacini* that we have named BnFMO. These studies reveal that this enzyme has a unique oligomeric structure, with lipid molecules observed at the trimeric interface. We have also determined that this enzyme can accept both 2,6-DHP and 2,6-DHNA as substrates. Further work will involve more detailed kinetic studies and the determination of the roles of active site residues in catalysis, which will provide more information on the molecular details of the BnFMO-catalyzed reaction.

■ ASSOCIATED CONTENT

Supporting Information

The Supporting Information is available free of charge at https://pubs.acs.org/doi/10.1021/acs.biochem.4c00306.

HPLC analysis of the BnFMO cofactor, BnFMO analytical ultracentrifugation results, BnFMO gel filtration chromatogram, ^{1}H and ^{13}C NMR spectra of 2,6-dihydroxynicotinic acid (2,6-DHNA) immediately after synthesis and after ∼ 100 h incubation, mass spectrometric analysis of the lipids associated with FMO, maps for the observed lipid density, BnFMO crystal structure images, cryo-EM data collection and refinement parameters, and crystal structure data collection and refinement parameters (PDF)

Accession Codes

The accession number for BnFMO is WP_063252926, and the UniProt ID is UP10007AB3525.

■ AUTHOR INFORMATION

Corresponding Author

Katherine A. Hicks − *Department of Chemistry, State University of New York at Cortland, Cortland, New York 13045, United States;* orcid.org/0000-0002-1474-1067; Email: katherine.hicks@cortland.edu

Authors

Brian C. Richardson − *The Hormel Institute, University of Minnesota, Austin, Minnesota 55912, United States*

Zachary R. Turlington − *Department of Chemistry, State University of New York at Cortland, Cortland, New York 13045, United States;* orcid.org/0000-0001-9560-0663

Sofia Vaz Ferreira de Macedo − *Department of Chemistry, State University of New York at Cortland, Cortland, New York 13045, United States*

Sara K. Phillips − *Department of Chemistry, State University of New York at Cortland, Cortland, New York 13045, United States*

Kay Perry − *NE-CAT and Department of Chemistry and Chemical Biology, Cornell University, Argonne National Laboratory, Argonne, Illinois 60439, United States*

Savannah G. Brancato − *Department of Chemistry, State University of New York at Cortland, Cortland, New York 13045, United States*

Emmalee W. Cooke − *Department of Chemistry, State University of New York at Cortland, Cortland, New York 13045, United States; Department of Chemistry, the College of Wooster, Wooster, Ohio 44691, United States*

Jonathan R. Gwilt − *Department of Chemistry, State University of New York at Cortland, Cortland, New York 13045, United States;* orcid.org/0009-0002-4815-0908

Morgan A. Dasovich − *Department of Chemistry, the College of Wooster, Wooster, Ohio 44691, United States*

Andrew J. Roering − *Department of Chemistry, State University of New York at Cortland, Cortland, New York 13045, United States*

Francis M. Rossi − *Department of Chemistry, State University of New York at Cortland, Cortland, New York 13045, United States*

Mark J. Snider − *Department of Chemistry, the College of Wooster, Wooster, Ohio 44691, United States;* orcid.org/0000-0003-1054-1276

Jarrod B. French − *The Hormel Institute, University of Minnesota, Austin, Minnesota 55912, United States;* orcid.org/0000-0002-6762-1309

Complete contact information is available at: https://pubs.acs.org/10.1021/acs.biochem.4c00306

Author Contributions

⊥B.C.R. and Z.R.T. contributed equally.

Funding

Research at SUNY Cortland was supported by NSF grant no. 1817633. Research at The College of Wooster was supported by NSF grant no. 1817535 and CHE-2017788. Research at the Hormel Institute was supported by the National Institutes of General Medical Sciences of the NIH under grant no. R35GM124898.

Notes

The authors declare no competing financial interest.

■ ACKNOWLEDGMENTS

This work is based upon research conducted at the Northeastern Collaborative Access Team beamlines, which are funded by the National Institute of General Medical Sciences from the National Institutes of Health (P30 GM124165). The Eiger 16M detector on the 24-1D-E beamline is funded by a NIH-ORIP HEI grant (S10OD021527). This research used resources of the Advanced Photon Source, a U.S. Department of Energy (DOE) Office of Science User Facility operated for the DOE Office of Science by Argonne National Laboratory under Contract no. DE-AC02-06CH11357. Crystallization screening at the National Crystallization Center at HWI was supported through the NIH grant R24M151256.

■ ABBREVIATIONS

6-HNA	6-hydroxynicotinic acid
2,6 DHP	2,6-dihydroxypyridine
2,4-DHBA	2,4-dihydroxybenzoic acid
2,6-DHNA	2,6-dihydroxynicotinic acid
IPTG	isopropyl β-D-thiogalactopyranoside
FAD	flavin adenine dinucleotide
FMN	flavin mononucleotide

NHACs	*N*-heterocyclic aromatic compounds
NADH	nicotinamide adenine dinucleotide (reduced form)
NAD^+	nicotinamide adenine dinucleotide (oxidized form)
FMO	flavin monooxygenase
FPLC	fast protein liquid chromatography
HPLC	high-pressure liquid chromatography
POPG	1-cis-9-octadecanoyl-2-cis-9-hexadecanoylphosphatidyl glycerol

REFERENCES

(1) Pašková, V.; Hilscherová, K.; Feldmannová, M.; Bláha, L. Toxic effects and oxidative stress in higher plants exposed to polycyclic aromatic hydrocarbons and their N-heterocyclic derivatives. *Environ. Toxicol. Chem.* **2006**, *25* (12), 3238−3245.

(2) Feldmannova, M.; Hilscherova, K.; Marsalek, B.; Blaha, L. Effects of N-heterocyclic polyaromatic hydrocarbons on survival, reproduction, and biochemical parameters in Daphnia magna. *Environ. Toxicol.* **2006**, *21* (4), 425−431.

(3) Bi, E.; Schmidt, T. C.; Haderlein, S. B. Environmental factors influencing sorption of heterocyclic aromatic compounds to soil. *Environ. Sci. Technol.* **2007**, *41* (9), 3172−3178.

(4) Buryskova, B.; Hilscherova, K.; Blaha, L.; Marsalek, B.; Holoubek, I. Toxicity and modulations of biomarkers in Xenopus laevis embryos exposed to polycyclic aromatic hydrocarbons and their N-heterocyclic derivatives. *Environ. Toxicol.* **2006**, *21* (6), 590−598.

(5) Kobeticova, K.; Bezchlebova, J.; Lana, J.; Sochova, I.; Hofman, J. Toxicity of four nitrogen-heterocyclic polyaromatic hydrocarbons (NPAHs) to soil organisms. *Ecotoxicol. Environ. Saf.* **2008**, *71* (3), 650−660.

(6) Guo, Y.; Li, D. F.; Ji, H.; Zheng, J.; Zhou, N. Y. Hexachlorobenzene Monooxygenase Substrate Selectivity and Catalysis: Structural and Biochemical Insights. *Appl. Environ. Microbiol.* **2020**, *87* (1), No. e01965-20.

(7) Pongpamorn, P.; Watthaisong, P.; Pimviriyakul, P.; Jaruwat, A.; Lawan, N.; Chitnumsub, P.; Chaiyen, P. Identification of a Hotspot Residue for Improving the Thermostability of a Flavin-Dependent Monooxygenase. *Chembiochem* **2019**, *20* (24), 3020−3031.

(8) Alhapel, A.; Darley, D. J.; Wagener, N.; Eckel, E.; Elsner, N.; Pierik, A. J. Molecular and functional analysis of nicotinate catabolism in Eubacterium barkeri. *Proc. Natl. Acad. Sci. U.S.A.* **2006**, *103* (33), 12341−12346.

(9) Kitts, C. L.; Schaechter, L. E.; Rabin, R. S.; Ludwig, R. A. Identification of cyclic intermediates in Azorhizobium caulinodans nicotinate catabolism. *J. Bacteriol.* **1989**, *171* (6), 3406−3411.

(10) Kitts, C. L.; Lapointe, J. P.; Lam, V. T.; Ludwig, R. A. Elucidation of the complete Azorhizobium nicotinate catabolism pathway. *J. Bacteriol.* **1992**, *174* (23), 7791−7797.

(11) Jiménez, J. I.; Canales, A.~.; Jiménez-Barbero, J.; Ginalski, K.; Rychlewski, L.; García, J. L.; Díaz, E. Deciphering the genetic determinants for aerobic nicotinic acid degradation: The nic cluster from Pseudomonas putida KT2440. *Proc. Natl. Acad. Sci. U.S.A.* **2008**, *105* (32), 11329−11334.

(12) Kincaid, V. A.; Sullivan, E. D.; Klein, R. D.; Noel, J. W.; Rowlett, R. S.; Snider, M. J. Structure and Catalytic Mechanism of Nicotinate (Vitamin B3) Degradative Enzyme Maleamate Amidohydrolase from Bordetella bronchiseptica RB50. *Biochemistry* **2012**, *51* (1), 545−554.

(13) Koser, S. A.; Baird, G. R. Bacterial Destruction of Nicotinic Acid. *J. Infect. Dis.* **1944**, *75* (3), 250−261.

(14) Ensign, J. C.; Rittenberg, S. C. The Pathway of Nicotinic Acid Oxidation by a Bacillus Species. *J. Biol. Chem.* **1964**, *239*, 2285−2291.

(15) Nagel, M. A.; Andreesen, J. Purification and characterization of the molybdoenzymes nicotinate dehydrogenase and 6-hydroxynicotinate dehydrogenase from Bacillus niacini. *Arch. Microbiol.* **1990**, *154*, 605−613.

(16) Hicks, K. A.; O'Leary, S. E.; Begley, T. P.; Ealick, S. E. Structural and Mechanistic Studies of HpxO, a Novel Flavin Adenine Dinucleotide-Dependent Urate Oxidase from *Klebsiella pneumoniae*. *Biochemistry* **2013**, *52* (3), 477−487.

(17) Bateman, A.; Martin, M. J.; Orchard, S.; Magrane, M.; Agivetova, R.; Ahmad, S.; Alpi, E.; Bowler-Barnett, E. H.; Britto, R.; Bursteinas, B.; et al. UniProt: the universal protein knowledgebase in 2021. *Nucleic Acids Res.* **2021**, *49* (D1), D480−D489.

(18) Schomburg, I.; Chang, A.; Ebeling, C.; Gremse, M.; Heldt, C.; Huhn, G.; Schomburg, D. BRENDA, the enzyme database: updates and major new developments. *Nucleic Acids Res.* **2004**, *32* (90001), D431−D433.

(19) Tanabe, M.; Kanehisa, M. Using the KEGG database resource. *Curr. Protoc. Bioinformatics*; Wiley, 2012; pp 1 12 11−11 12 43. Chapter 1.

(20) Hicks, K. A.; Yuen, M. E.; Zhen, W. F.; Gerwig, T. J.; Story, R. W.; Kopp, M. C.; Snider, M. J. Structural and Biochemical Characterization of 6-Hydroxynicotinic Acid 3-Monooxygenase, A Novel Decarboxylative Hydroxylase Involved in Aerobic Nicotinate Degradation. *Biochemistry* **2016**, *55* (24), 3432−3446.

(21) Nakamoto, K. D.; Perkins, S. W.; Campbell, R. G.; Bauerle, M. R.; Gerwig, T. J.; Gerislioglu, S.; Wesdemiotis, C.; Anderson, M. A.; Hicks, K. A.; Snider, M. J. Mechanism of 6-Hydroxynicotinate 3-Monooxygenase, a Flavin-Dependent Decarboxylative Hydroxylase Involved in Bacterial Nicotinic Acid Degradation. *Biochemistry* **2019**, *58* (13), 1751−1763.

(22) Perkins, S. W.; Hlaing, M. Z.; Hicks, K. A.; Rajakovich, L. J.; Snider, M. J. Mechanism of the Multistep Catalytic Cycle of 6-Hydroxynicotinate 3-Monooxygenase Revealed by Global Kinetic Analysis. *Biochemistry* **2023**, *62* (10), 1553−1567.

(23) van Berkel, W. J. H.; Kamerbeek, N. M.; Fraaije, M. W. Flavoprotein monooxygenases, a diverse class of oxidative biocatalysts. *J. Biotechnol.* **2006**, *124* (4), 670−689.

(24) Huijbers, M. M. E.; Montersino, S.; Westphal, A. H.; Tischler, D.; van Berkel, W. J. H. Flavin dependent monooxygenases. *Arch. Biochem. Biophys.* **2014**, *544* (0), 2−17.

(25) Harvey, Z. H.; Snider, M. J. Draft Genome Sequence of the Nicotinate-Metabolizing Soil Bacterium Bacillus niacini DSM 2923. *Genome Announc.* **2014**, *2* (6), No. e01251-14.

(26) Punjani, A.; Rubinstein, J. L.; Fleet, D. J.; Brubaker, M. A. cryoSPARC: algorithms for rapid unsupervised cryo-EM structure determination. *Nat. Methods* **2017**, *14* (3), 290−296.

(27) Williams, C. J.; Headd, J. J.; Moriarty, N. W.; Prisant, M. G.; Videau, L. L.; Deis, L. N.; Verma, V.; Keedy, D. A.; Hintze, B. J.; Chen, V. B.; Jain, S.; Lewis, S. M.; Arendall, W. B., 3rd; Snoeyink, J.; Adams, P. D.; Lovell, S. C.; Richardson, J. S.; Richardson, D. C. MolProbity: More and better reference data for improved all-atom structure validation. *Protein Sci.* **2018**, *27* (1), 293−315.

(28) Barad, B. A.; Echols, N.; Wang, R. Y.; Cheng, Y.; DiMaio, F.; Adams, P. D.; Fraser, J. S. EMRinger: side chain-directed model and map validation for 3D cryo-electron microscopy. *Nat. Methods* **2015**, *12* (10), 943−946.

(29) Pettersen, E. F.; Goddard, T. D.; Huang, C. C.; Couch, G. S.; Greenblatt, D. M.; Meng, E. C.; Ferrin, T. E. UCSF Chimera–a visualization system for exploratory research and analysis. *J. Comput. Chem.* **2004**, *25* (13), 1605−1612.

(30) Marchler-Bauer, A.; Bo, Y.; Han, L.; He, J.; Lanczycki, C. J.; Lu, S.; Chitsaz, F.; Derbyshire, M. K.; Geer, R. C.; Gonzales, N. R.; Gwadz, M.; Hurwitz, D. I.; Lu, F.; Marchler, G. H.; Song, J. S.; Thanki, N.; Wang, Z.; Yamashita, R. A.; Zhang, D.; Zheng, C.; Geer, L. Y.; Bryant, S. H. CDD/SPARCLE: functional classification of proteins via subfamily domain architectures. *Nucleic Acids Res.* **2017**, *45* (D1), D200−D203.

(31) Detmer, K.; Massey, V. Effect of monovalent anions on the mechanism of phenol hydroxylase. *J. Biol. Chem.* **1984**, *259* (18), 11265−11272.

(32) Steennis, P. J.; Cordes, M. M.; Hilkens, J. G.; Muller, F. On the interaction of para-hydroxybenzoate hydroxylase from Pseudomonas fluorescens with halogen ions. *FEBS Lett.* **1973**, *36* (2), 177−180.

https://doi.org/10.1021/acs.biochem.4c00306
Biochemistry 2024, 63, 2506−2516

(33) Paul, C. E.; Eggerichs, D.; Westphal, A. H.; Tischler, D.; van Berkel, W. J. H. Flavoprotein monooxygenases: Versatile biocatalysts. *Biotechnol. Adv.* **2021**, *51*, 107712.
(34) Schreuder, H. A.; Mattevi, A.; Obmolova, G.; Kalk, K. H.; Hol, W. G.; van der Bolt, F. J.; van Berkel, W. J. Crystal structures of wild-type p-hydroxybenzoate hydroxylase complexed with 4-amino-benzoate,2,4-dihydroxybenzoate, and 2-hydroxy-4-aminobenzoate and of the Tyr222Ala mutant complexed with 2-hydroxy-4-amino-benzoate. Evidence for a proton channel and a new binding mode of the flavin ring. *Biochemistry* **1994**, *33* (33), 10161−10170.
(35) Schreuder, H. A.; Prick, P. A.; Wierenga, R. K.; Vriend, G.; Wilson, K. S.; Hol, W. G.; Drenth, J. Crystal structure of the p-hydroxybenzoate hydroxylase-substrate complex refined at 1.9 Å resolution. *J. Mol. Biol.* **1989**, *208* (4), 679−696.
(36) Wang, J.; Ortiz-Maldonado, M.; Entsch, B.; Massey, V.; Ballou, D.; Gatti, D. L. Protein and ligand dynamics in 4-hydroxybenzoate hydroxylase. *Proc. Natl. Acad. Sci. U.S.A.* **2002**, *99* (2), 608−613.
(37) Krissinel, E.; Henrick, K. Inference of macromolecular assemblies from crystalline state. *J. Mol. Biol.* **2007**, *372* (3), 774−797.
(38) McCulloch, K. M.; Mukherjee, T.; Begley, T. P.; Ealick, S. E. Structure of the PLP Degradative Enzyme 2-Methyl-3-hydroxypyridine-5-carboxylic Acid Oxygenase from Mesorhizobium loti MAFF303099 and Its Mechanistic Implications. *Biochemistry* **2009**, *48* (19), 4139−4149.
(39) Montersino, S.; Te Poele, E.; Orru, R.; Westphal, A. H.; Barendregt, A.; Heck, A. J. R.; van der Geize, R.; Dijkhuizen, L.; Mattevi, A.; van Berkel, W. J. H. 3-Hydroxybenzoate 6-Hydroxylase from Rhodococcus jostii RHA1 Contains a Phosphatidylinositol Cofactor. *Front. Microbiol.* **2017**, *8*, 1110.
(40) Kachalova, G. S.; Bourenkov, G. P.; Mengesdorf, T.; Schenk, S.; Maun, H. R.; Burghammer, M.; Riekel, C.; Decker, K.; Bartunik, H. D. Crystal structure analysis of free and substrate-bound 6-hydroxy-L-nicotine oxidase from Arthrobacter nicotinovorans. *J. Mol. Biol.* **2010**, *396* (3), 785−799.
(41) Montersino, S.; Orru, R.; Barendregt, A.; Westphal, A. H.; van Duijn, E.; Mattevi, A.; van Berkel, W. J. H. Crystal Structure of 3-Hydroxybenzoate 6-Hydroxylase Uncovers Lipid-assisted Flavoprotein Strategy for Regioselective Aromatic Hydroxylation. *J. Biol. Chem.* **2013**, *288* (36), 26235−26245.
(42) Kachalova, G.; Decker, K.; Holt, A.; Bartunik, H. D. Crystallographic snapshots of the complete reaction cycle of nicotine degradation by an amine oxidase of the monoamine oxidase (MAO) family. *Proc. Natl. Acad. Sci. U.S.A.* **2011**, *108* (12), 4800−4805.
(43) Pintilie, G. Diagnosing and treating issues in cryo-EM map-derived models. *Structure* **2023**, *31* (7), 759−761.
(44) Frieden, C. Protein oligomerization as a metabolic control mechanism: Application to apoE. *Protein Sci.* **2019**, *28* (4), 837−842.
(45) Aloh, C. H.; Zeczycki, T. N.; Ellis, H. R. Oligomeric Changes Regulate Flavin Transfer in Two-Component FMN Reductases Involved in Sulfur Metabolism. *Biochemistry* **2023**, *62* (18), 2751−2762.
(46) Gatti, D. L.; Entsch, B.; Ballou, D. P.; Ludwig, M. L. pH-dependent structural changes in the active site of p-hydroxybenzoate hydroxylase point to the importance of proton and water movements during catalysis. *Biochemistry* **1996**, *35* (2), 567−578.
(47) Hiromoto, T.; Fujiwara, S.; Hosokawa, K.; Yamaguchi, H. Crystal structure of 3-hydroxybenzoate hydroxylase from Comamonas testosteroni has a large tunnel for substrate and oxygen access to the active site. *J. Mol. Biol.* **2006**, *364* (5), 878−896.
(48) Entsch, B.; Palfey, B. A.; Ballou, D. P.; Massey, V. Catalytic function of tyrosine residues in para-hydroxybenzoate hydroxylase as determined by the study of site-directed mutants. *J. Biol. Chem.* **1991**, *266* (26), 17341−17349.
(49) Manenda, M. S.; Picard, M. E.; Zhang, L.; Cyr, N.; Zhu, X.; Barma, J.; Pascal, J. M.; Couture, M.; Zhang, C.; Shi, R. Structural analyses of the Group A flavin-dependent monooxygenase PieE reveal a sliding FAD cofactor conformation bridging OUT and IN conformations. *J. Biol. Chem.* **2020**, *295* (14), 4709−4722.
(50) Ballou, D. P.; Entsch, B.; Cole, L. J. Dynamics involved in catalysis by single-component and two-component flavin-dependent aromatic hydroxylases. *Biochem. Biophys. Res. Commun.* **2005**, *338* (1), 590−598.
(51) Eppink, M. H. M.; Bunthof, C.; Schreuder, H. A.; van Berkel, W. J. Phe161 and Arg166 variants of p-hydroxybenzoate hydroxylase. Implications for NADPH recognition and structural stability. *FEBS Lett.* **1999**, *443* (3), 251−255.
(52) Eppink, M. H.; Schreuder, H. A.; van Berkel, W. J. Lys42 and Ser42 variants of p-hydroxybenzoate hydroxylase from Pseudomonas fluorescens reveal that Arg42 is essential for NADPH binding. *Eur. J. Biochem.* **1998**, *253* (1), 194−201.
(53) Holm, L. Using Dali for Protein Structure Comparison. *Methods Mol. Biol.* **2020**, *2112*, 29−42.
(54) Chen, Q.; Huang, Y.; Duan, Y.; Li, Z.; Cui, Z.; Liu, W. Crystal structure of p-nitrophenol 4-monooxygenase PnpA from Pseudomonas putida DLL-E4: The key enzyme involved in p-nitrophenol degradation. *Biochem. Biophys. Res. Commun.* **2018**, *504* (4), 715−720.
(55) Weiss, A. K. H.; Naschberger, A.; Loeffler, J. R.; Gstach, H.; Bowler, M. W.; Holzknecht, M.; Cappuccio, E.; Pittl, A.; Etemad, S.; Dunzendorfer-Matt, T.; Scheffzek, K.; Liedl, K. R.; Jansen-Durr, P. Structural basis for the bi-functionality of human oxaloacetate decarboxylase FAHD1. *Biochem. J.* **2018**, *475* (22), 3561−3576.
(56) Pang, A. H.; Garneau-Tsodikova, S.; Tsodikov, O. V. Crystal structure of halogenase PltA from the pyoluteorin biosynthetic pathway. *J. Struct. Biol.* **2015**, *192* (3), 349−357.
(57) Padyana, A. K.; Gross, S.; Jin, L.; Cianchetta, G.; Narayanaswamy, R.; Wang, F.; Wang, R.; Fang, C.; Lv, X.; Biller, S. A.; Dang, L.; Mahoney, C. E.; Nagaraja, N.; Pirman, D.; Sui, Z.; Popovici-Muller, J.; Smolen, G. A. Structure and inhibition mechanism of the catalytic domain of human squalene epoxidase. *Nat. Commun.* **2019**, *10* (1), 97.
(58) Oke, M.; Carter, L. G.; Johnson, K. A.; Liu, H.; McMahon, S. A.; Yan, X.; Kerou, M.; Weikart, N. D.; Kadi, N.; Sheikh, M. A.; Schmelz, S.; Dorward, M.; Zawadzki, M.; Cozens, C.; Falconer, H.; Powers, H.; Overton, I. M.; van Niekerk, C. A.; Peng, X.; Patel, P.; Garrett, R. A.; Prangishvili, D.; Botting, C. H.; Coote, P. J.; Dryden, D. T.; Barton, G. J.; Schwarz-Linek, U.; Challis, G. L.; Taylor, G. L.; White, M. F.; Naismith, J. H. The Scottish Structural Proteomics Facility: targets, methods and outputs. *J. Struct. Funct. Genomics* **2010**, *11* (2), 167−180.
(59) Zhang, S.; Sakuma, M.; Deora, G. S.; Levy, C. W.; Klausing, A.; Breda, C.; Read, K. D.; Edlin, C. D.; Ross, B. P.; Wright Muelas, M.; Day, P. J.; O'Hagan, S.; Kell, D. B.; Schwarcz, R.; Leys, D.; Heyes, D. J.; Giorgini, F.; Scrutton, N. S. A brain-permeable inhibitor of the neurodegenerative disease target kynurenine 3-monooxygenase prevents accumulation of neurotoxic metabolites. *Commun. Biol.* **2019**, *2*, 271.
(60) Treiber, N.; Schulz, G. E. Structure of 2,6-Dihydroxypyridine 3-hydroxylase from a Nicotine-degrading Pathway. *J. Mol. Biol.* **2008**, *379* (1), 94−104.
(61) Entsch, B.; Ballou, D. P.; Husain, M.; Massey, V. Catalytic mechanism of p-hydroxybenzoate hydroxylase with p-mercaptobenzoate as substrate. *J. Biol. Chem.* **1976**, *251* (23), 7367−7379.

NOTE ADDED AFTER ASAP PUBLICATION

This paper was published ASAP on September 11, 2024. Updates have been made to the Results and Discussion section, the caption of Figure 6, and the Supporting Information file. The updated version was reposted on September 13, 2024.

https://doi.org/10.1021/acs.biochem.4c00306
Biochemistry 2024, 63, 2506−2516